

Implications of Recent Observational Discoveries for the Nature and Origin of Gamma-Ray Bursts

D. Q. Lamb

Department of Astronomy & Astrophysics, University of Chicago, Chicago, IL 60637, U.S.A.

Abstract

The discoveries that GRBs have X-ray, optical and radio afterglows have connected the study of GRBs to the rest of astronomy, and revolutionized the field. In this review, I discuss the implications that the observation of these afterglows have for burst energies and luminosities, and for models of the bursts and their afterglows. I describe recent evidence linking the long, softer, smoother GRBs detected by BeppoSAX and core collapse supernovae. Finally, I summarize recent work showing that, if these GRBs are due to the collapse of massive stars, they may provide a powerful probe of the very high redshift universe.

Key words: Gamma rays: bursts

1 Introduction

Gamma-ray bursts (GRBs) were discovered serendipitously more than a quarter century ago [1]. The bursts consist of short, intense episodes of gamma-ray emission, lasting anywhere from $\sim 10^{-2}$ seconds to $\sim 10^3$ seconds. The time histories of GRBs are diverse, as Figure 1 illustrates. However, studies of the time histories have shown that the bursts can be separated into two classes: short, harder, more variable bursts; and long, softer, smoother bursts [3,4] (see Figure 2). Burst spectra are nonthermal; the photon number spectrum is a broken power law, with average slopes ~ -1.5 and ~ -2.5 at low and high energies and a shoulder at 100 keV - 1 MeV [5,6].

¹ E-mail: lamb@oddjob.uchicago.edu

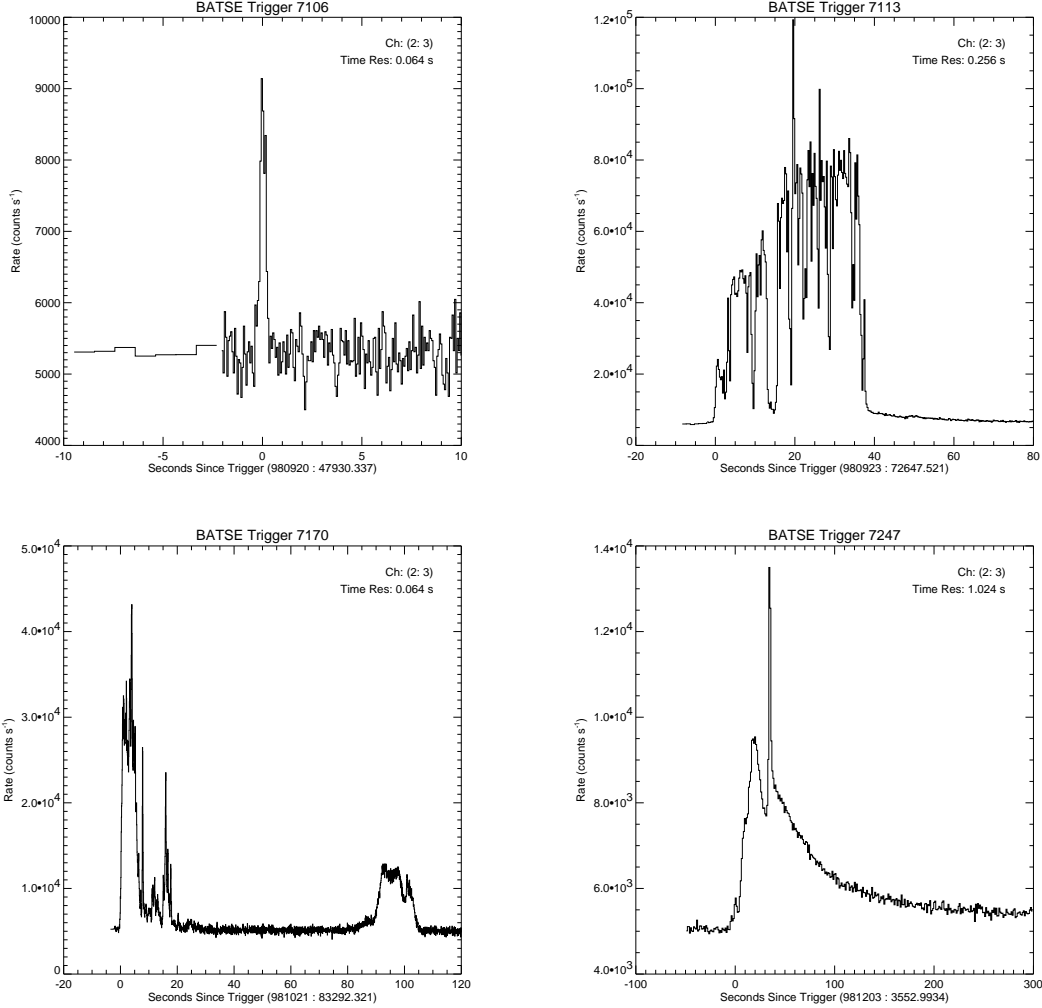


Fig. 1. Four GRB time histories of GRBs 980920, 980923, 981021, and 981203. These four bursts occurred within about two months, illustrating the diversity of GRB time histories. [2]

The data gathered by the Burst and Transient Source Experiment (BATSE) on the *Compton* Gamma-Ray Observatory confirmed earlier evidence of a rollover in the cumulative brightness distribution of GRBs, showing that the burst sources are inhomogeneously distributed in space [7]. The data also showed that the sky distribution of even faint bursts is consistent with isotropy [7] (see Figure 3). This combination of results implies that we are at, or near, the center of the spatial distribution of burst sources and that the intrinsic brightness and/or spatial density of the sources decreases with increasing distance from us.

The BATSE results showed that the bursts cannot come from a population of neutron stars in a thick Galactic disk (as was previously thought) and spurred interest in the possibility that the sources of the bursts lie at cosmological distances. Yet the evidence remained circumstantial. Consequently, the GRB distance scale – and even more, the nature of the burst sources – was debat-

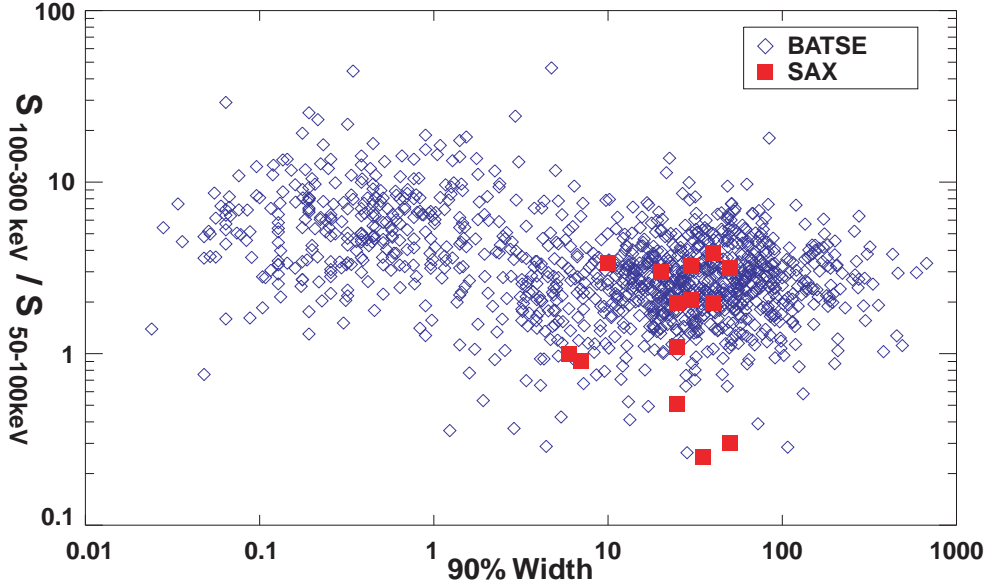


Fig. 2. Distribution of duration (as measured by the time interval containing 90% of the photon counts) versus spectral hardness (as measured by the ratio of fluence in the 50 - 100 keV and 100 - 300 keV energy bands) for bursts in the BATSE 4B catalog [2] (diamonds), showing clear evidence for two classes of bursts: short, harder, more variable bursts; and long, softer, smoother bursts. Events detected by BeppoSAX (solid squares) belong to the latter class. From [13].

able [8,9]. The principal reason for the continuing uncertainty in the distance scale of the bursts was that no definite counterpart to any burst could be found at other wavelengths, despite intense efforts spanning more than two decades. Consequently, the study of GRBs was isolated from the rest of astronomy. Scientists studying them had only the laws of physics and the properties of the bursts themselves to guide them in attempting to solve the GRB mystery.

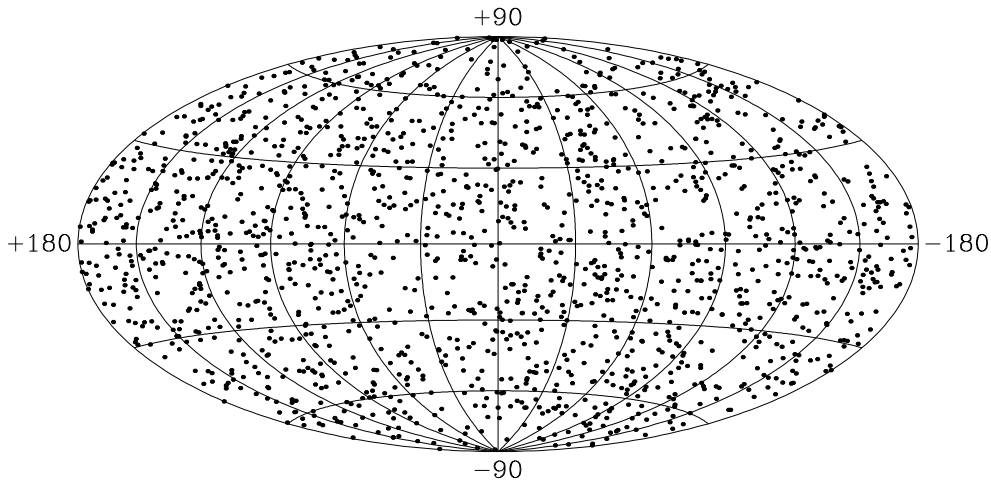


Fig. 3. The positions in Galactic coordinates of the GRBs in the BATSE 4B catalog [2], showing the isotropy of the burst sky distribution [7].

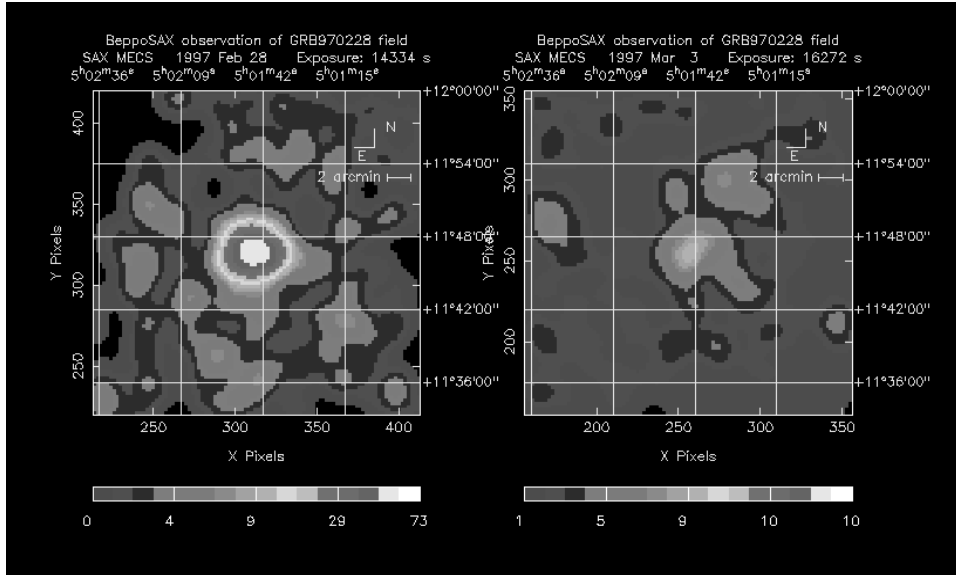


Fig. 4. BeppoSAX observations of the fading X-ray afterglow of GRB 970228. Left panel: MECS image on February 28. Right panel: a deeper MECS image on March 3 [14]

The relatively accurate ($3'$) gamma-ray burst positions found using BeppoSAX, and disseminated within a day or so, revolutionized the field. They led to the remarkable discoveries that GRBs have X-ray [10], optical [11] and radio [12] afterglows, finally connecting the study of GRBs with the rest of astronomy. The breakthroughs in our understanding of GRBs made possible by these discoveries cannot be overstated.

In this review, dedicated to the memory of my friend and colleague David Schramm, I describe these recent breakthroughs. I first relate the discovery of

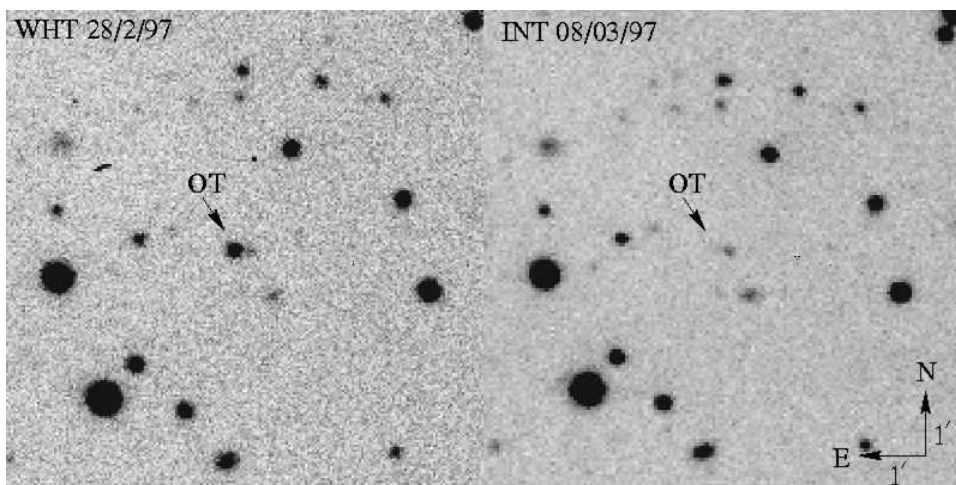


Fig. 5. William Herschel Telescope images taken on February 28 and March 8 of the fading optical afterglow of GRB 970228. [11]



Fig. 6. HST STIS image taken on September 4 of the optical afterglow of GRB 970228, which revealed the presence of a faint ($R = 25.5$) host galaxy. Both are clearly visible near the center of the WFPC2 image [15].

GRB X-ray, optical and radio afterglows. I then discuss the implications that the observations of these afterglows have for burst energies and luminosities, and for models of the bursts and their afterglows. I describe recent evidence linking GRBs and core collapse supernovae. Finally, I summarize recent work showing that, if GRBs are due to the collapse of massive stars, GRBs may provide a powerful probe of the very high redshift universe.

2 Recent Discoveries

Following the detection of GRB 970228 by BeppoSAX, follow-up observations revealed a fading X-ray source coincident with the position of the GRB [10] (see Figure 4). The relatively rapid dissemination of this position led to the

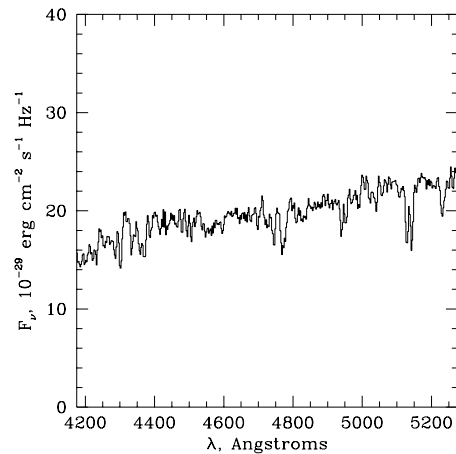


Fig. 7. Absorption lines of [Mg II] 5130 and 5144 Å and [Fe II] 4770 Å, among others, at a redshift $z = 0.83$ in the spectrum of the optical afterglow of GRB 970508, showing that the burst occurred at this redshift or larger. [16]

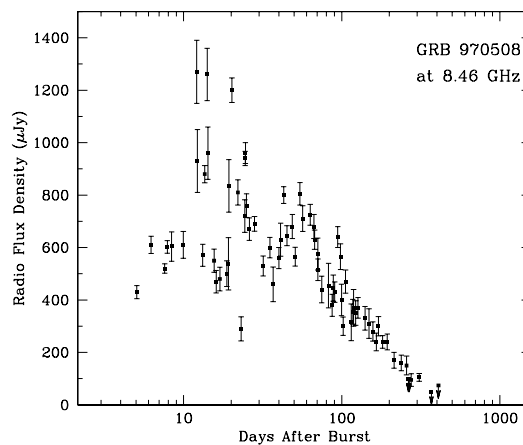


Fig. 8. Radio observations of the afterglow of GRB 970508. The rapid variability seen at early times disappears after ≈ 30 days. This behavior has been interpreted as due to scintillation, implying that GRB sources are highly compact and expand at relativistic speeds [12].

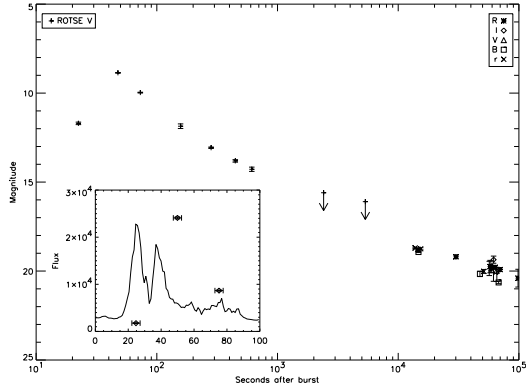


Fig. 9. ROTSE observations of bright ($m_V \approx 9$) optical emission coincident with GRB 990123. The inset shows the BATSE time history of the burst and three of the ROTSE data points (arbitrarily scaled to the BATSE time history) [17].

discovery of a fading optical source coincident with the X-ray source [11] (see Figure 5), establishing that GRBs exhibit both X-ray and optical afterglows. Subsequent observations using the Hubble Space Telescope revealed a faint ($R = 25.5$) underlying galaxy [15] (see Figure 6).

Two months later, Metzger et al. [16] found redshifted absorption lines of Mg II and Fe II at $z = 0.83$ in the optical spectrum of the GRB 970508 afterglow (see Figure 7), which established that most (perhaps all) GRB sources lie at cosmological distances. At about the same time, Frail et al. [12] discovered a radio source coincident with the fading X-ray afterglow of this burst, marking the first detection of a radio afterglow. The radio afterglow showed rapid variability, which disappeared after about 30 days (see Figure 8). The rapid variability has been interpreted as due to scintillation, implying that GRB sources are highly compact and expand at relativistic speeds [12].

Finally, we now know that GRBs can produce astonishingly bright optical emission coincident with the burst itself. ROTSE, a robotic optical telescope, slewed to the position of GRB 990123, a burst whose position was determined by BATSE and disseminated by the Gamma-Ray Burst Coordinate Network (GCN), within ≈ 20 seconds of the onset of the burst. The ROTSE observations revealed intense optical emission, peaking at $m_V \approx 9$ during the burst and fading thereafter [17] (see Figure 9).

X-ray afterglows are now known for about two dozen GRBs [18]. Optical afterglows have been detected for roughly half of these bursts [13], and radio afterglows have been detected for about one third of them [19]. Host galaxies have been found for most of the bursts with detected optical and/or radio afterglows [13]. Redshifts are known for eight GRBs, three of these are from spectroscopic observations of the optical afterglow, and the remainder are from spectroscopic observations of the host galaxy (see Table 1).

Not so long ago, adherents of the cosmological hypothesis for GRBs favored a redshift range $0.1 \lesssim z \lesssim 1$, which was derived primarily from the brightness distribution of the bursts under the assumption that GRBs are standard

candles (see, e.g., [27]). Now astrophysicists routinely talk about redshift distances $1 \lesssim z \lesssim 6$, a redshift range that is consistent with the modest number of GRB redshifts that have been determined so far (see, e.g., [28–31]). The increase in the GRB distance scale implies that the GRB phenomenon is much rarer than was previously thought. For example, Schmidt [32] finds that the GRB rate must be

$$R_{\text{GRB}} \sim 10^{-10} \text{ GRBs yr}^{-1} \text{ Mpc}^{-3} \quad (1)$$

in order both to match the brightness distribution of the BATSE bursts and to accommodate the redshift distance of $z = 3.42$ inferred for GRB 971214.

By comparison, the rates of neutron star-neutron star (NS-NS) binary mergers [29] and the rate of Type Ib-Ic supernovae [33] are

$$R_{\text{NS-NS}} \sim 10^{-6} \text{ mergers yr}^{-1} \text{ Mpc}^{-3} \quad (2)$$

$$R_{\text{Type Ib-Ic}} \sim 3 \times 10^{-5} \text{ SNe yr}^{-1} \text{ Mpc}^{-3} . \quad (3)$$

The rate of neutron star-black hole (NS-BH) binary mergers will be smaller. Nevertheless, it is clear that, if either of these events are the sources of GRBs, only a tiny fraction of them produce an observable GRB. Even if one posits strong collimation (i.e., $f_{\text{jet}} \approx 10^{-2}$), the fraction is small:

$$R_{\text{GRB}}/R_{\text{NS-NS}} \sim 10^{-2} (f_{\text{jet}}/10^{-2})^{-1} \quad (4)$$

$$R_{\text{GRB}}/R_{\text{Type Ib-Ic}} \sim 3 \times 10^{-4} (f_{\text{jet}}/10^{-2})^{-1} . \quad (5)$$

Therefore, if such events are the sources of GRBs, either the bursts are very strongly collimated ($f_{\text{jet}} \sim 10^{-6} - 10^{-4}$) or the physical conditions necessary to produce bursts are rarely satisfied in binary mergers and/or the core collapse of massive stars, implying that the GRB phenomenon is not robust [34].

3 Burst Energies and Luminosities

Table 1 lists isotropic-equivalent luminosities and energies of the bursts for which this information is known. The maximum energy $(E_{\text{GRB}})_{\text{max}}$ that has been observed for a GRB imposes an important requirement on GRB models, and is therefore of great interest to theorists. The current record holder is GRB 990123 at $z = 1.6$, which implies $E_{\text{GRB}} \sim 2 \times 10^{54} f_{\text{jet}}$ erg from its gamma-ray fluence, assuming $\Omega_M = 0.3$ and $\Omega_\Lambda = 0.7$ [21]. Even if GRBs are

Table 1

Peak Photon Fluxes and Isotropic Luminosities for GRBs with Known Redshifts

GRB	Redshift	P (ph cm ⁻² s ⁻¹) ^a	L_P (ph s ⁻¹) ^b	Redshift Reference
970228	0.695	3.5	5.1×10^{57}	[20]
970508	0.835	1.2	2.5×10^{57}	[16]
971214	3.418	2.3	6.4×10^{58}	[21]
980613	1.096	0.63	2.3×10^{57}	[22]
980703	0.967	2.6	7.4×10^{57}	[23]
990123	1.600	16.4	1.2×10^{59}	[24]
990510	1.619	8.16	6.2×10^{58}	[25]
990712 ^c	0.430	–	–	[26]

^a From J. Norris (<http://coss.gsfc.nasa.gov/coss/batse/counterparts>). The listed peak photon flux is that in the energy band 50 - 300 keV.

^b Assuming $H_0 = 65$ km s⁻¹ Mpc⁻¹, $\Omega_M = 0.3$, and $\Omega_\Lambda = 0.7$.

^c Peak photon flux not yet reported.

strongly collimated, they are still far and away the brightest electromagnetic phenomenon in the Universe, as the following comparison illustrates:

- $L_{\text{SNe}} \lesssim 10^{44}$ erg s⁻¹
- $L_{\text{SGR}} \lesssim 10^{45}$ erg s⁻¹
- $L_{\text{AGN}} \lesssim 10^{45}$ erg s⁻¹
- $L_{\text{GRB}} \sim 10^{51} (f_{\text{jet}}/10^{-2})$ erg s⁻¹

The luminosities of the GRBs listed in Table 1 span a factor of more than one hundred; i.e., $\Delta L_{\text{GRB}}/L_{\text{GRB}} \gtrsim 10^2$. Thus (if there was previously any doubt), determination of the redshift distances of a modest number of GRBs has put to rest once and for all the idea that GRBs are “standard candles.” The extensive studies by Loredo and Wasserman [35,36] and the study by Schmidt [32] show that the luminosity function for GRBs could well be much broader.

Even taking a luminosity range $\Delta L_{\text{GRB}}/L_{\text{GRB}} \gtrsim 10^2$ implies that $\Delta F_{\text{GRB}}/F_{\text{GRB}} \gtrsim 10^4$, given the range in the distances of the GRBs whose redshifts are currently known. This is far broader than the range of GRB peak fluxes in the BATSE 4B catalog [2], and implies that the flux distribution of the bursts extends well below the BATSE threshold.

The breadth of the GRB luminosity function and the narrow range in GRB distances due to cosmology (wasserman92,lamb99b) suggests that a large part of the differences between apparently bright and apparently dim bursts (such as time stretching of burst peaks [39–41], decreased variability [42], and spectral softening [43]) are due to *intrinsic* differences between *intrinsically* bright and faint bursts, rather than to, e.g., cosmological time dilation [34].

4 Burst Models

The most widely discussed models of the sources of GRBs involve a black hole and an accretion disk, formed either through the core collapse of a massive star [44–50] or the coalescence of a neutron star – neutron star (NS-NS) or neutron star – black hole (NS-BH) binary [51–53]. The former are expected to occur near or in the star-forming regions of their host galaxies, while most of the latter are expected to occur outside of the galaxies in which they were born.

The energies listed in Table 1 are difficult to accommodate in NS-NS or NS-BH binary merger models without invoking strong collimation of the burst. Core collapse (so-called “collapsar”) models can accommodate such energies more easily, although energies $\gtrsim 10^{54}$ erg require collimation, even assuming a high efficiency for the conversion of gravitational binding energy into gamma-rays [54].

Current models of the bursts themselves fall into three general categories: Those that invoke a central engine, those that invoke internal shock waves in a relativistically expanding outflow, and those that invoke a relativistic external shock wave. Dermer [55] argues that the external shock wave model explains many of the observed properties of the bursts. By contrast, Fenimore [56] argues that several features of GRBs, such as the large gaps seen in burst time histories, cannot be explained by the external shock wave model, and that the bursts must therefore be due either to a central engine or to internal shocks in a relativistically expanding wind. Either way, the intensity and spectral variations seen during the burst must originate at a central engine. This implies that the lifetime of the central engine must in many cases be $t_{\text{engine}} \gtrsim 100 - 1000$ s, which poses a severe difficulty for NS-NS or NS-BH binary merger models, if such models are invoked to explain the long, softer, smoother bursts.

5 Afterglow Models

The most widely discussed model of GRB afterglows is the fireball model, in which the energy released by the central engine leads to a relativistic shock wave that expands into the interstellar medium or into material lost earlier by the burst progenitor via its stellar wind [57,58]. As the ejected material encounters the ambient material, two shocks are produced: A short-lived reverse shock that travels through the ejected material and a long-lived forward shock that propagates into the swept-up ambient material. In the fireball model, the afterglow emission at radio, optical and X-ray energies is produced by synchrotron emission. This requires (1) efficient transfer of energy from the

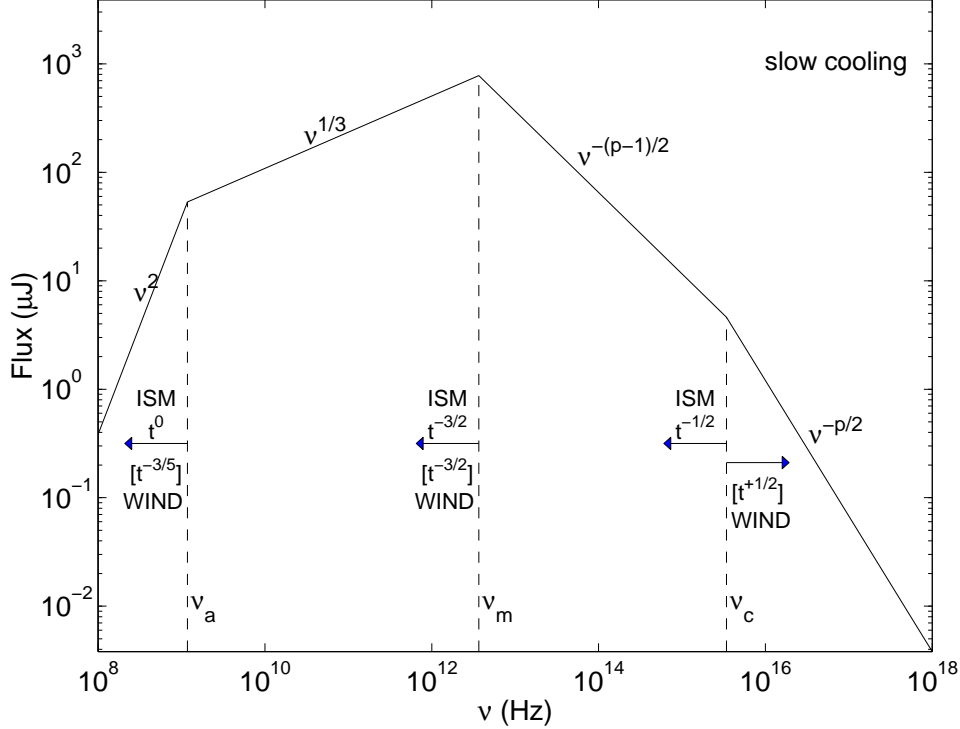


Fig. 10. Afterglow spectrum expected in the relativistic external shock model. The spectrum resembles a broken power-law with four segments (see text). The segments are separated by three frequencies: ν_a , the synchrotron self-absorption frequency; ν_m , the frequency of the synchrotron peak, which corresponds to the minimum energy of the electrons; and ν_c , which corresponds to the energy of the electrons that have begun to cool significantly. Note the distinctly different evolution with time of ν_a and ν_c in the ISM and progenitor wind models. From [13].

shocked protons (which contain most of the energy) to the electrons; (2) efficient acceleration of the electrons to high energies; and (3) rapid growth of the magnetic field to values corresponding to energy densities $\sim 10^{-2}$ of that of the protons.

Figure 10 shows the afterglow spectrum expected in the relativistic fireball model. The spectrum resembles a broken power-law with four segments, which are due to self-absorbed synchrotron emission at radio energies (segment 1); optically thin synchrotron emission extending from sub-millimeter through the optical into the UV, with the synchrotron peak in the near IR or optical (segments 2 and 3); and synchrotron emission above the synchrotron peak from electrons that have already cooled (segment 4). The four broken power-law segments are separated by three frequencies: ν_a , the synchrotron self-absorption frequency; ν_m , the frequency of the synchrotron peak, which corresponds to the minimum energy of the electrons; and ν_c , which corresponds to the energy of the electrons that have begun to cool significantly.

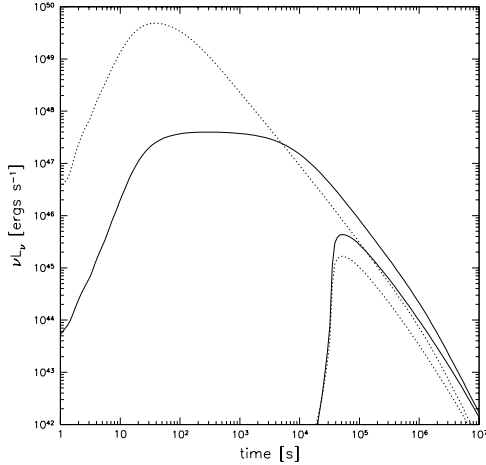


Fig. 11. Calculations of afterglow light curves for isotropic-equivalent energy $E_0 = 10^{54}$ ergs s $^{-1}$, $\Gamma_0 = 300$ and $\theta_{jet,0} = 0.2$ radians. The dotted lines are the X-ray light curves and the solid lines are the optical light curves. The thick lines are for $\theta_{obs} = 0^\circ$ while the thin lines are for $\theta_{obs} = 16^\circ$ [63].

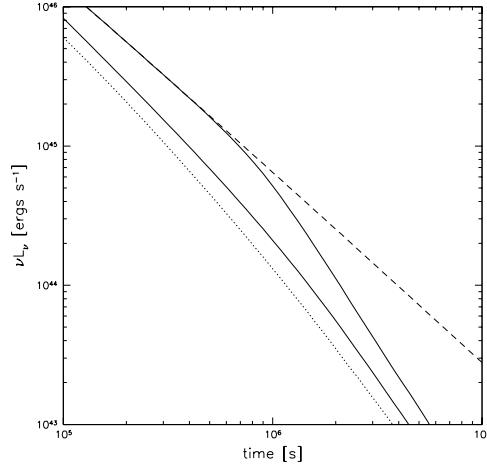


Fig. 12. Calculations of afterglow light curves in the time range where the beaming effects are strongest. The thin solid line is for $\theta_{jet} = \theta_{jet,0} = 0.2$ radians; the thick solid line is for $\theta_{jet} = \theta_{jet,0} + 1/\sqrt{3}\Gamma$; the dotted line is for $\theta_{jet} = \theta_{jet,0} + 1/\Gamma$; and the dashed line is for $\theta_{jet} = \pi$ (spherical case) [63].

The evolution of the frequencies ν_a and ν_c are distinctly different, depending on whether the relativistic fireball is expanding into a constant density ISM, or into the decreasing density $\rho \sim r^{-2}$ expected for material previously ejected by the stellar wind of the progenitor of the GRB [59] (see Figure 10).

If the relativistic fireball model suffices to explain burst afterglows, much can be learned (in principle), including the isotropic-equivalent energy of the fireball, the ratio of the energy in the magnetic field to that in relativistic electrons, and the density of the external medium into which the fireball expands (see, e.g., [30,60]). This requires, however, enough simultaneous broad-band photometric or spectral observations to determine accurately the frequencies ν_a, ν_m , and ν_c . It should also be possible, in principle, to use the effects of extinction due to dust and absorption above the Lyman limit due to hydrogen in the host galaxy to determine the redshift of the burst itself, but so far, this goal has eluded modelers (see, e.g, [60]).

6 Beaming

Many powerful astrophysical sources produce jets, including young protostars; so-called “microquasars,” which are black hole binaries in the Galaxy; radio galaxies; and active galactic nuclei. There is also evidence from polarization

observations that some supernovae are asymmetric [61]. Most theorists therefore now expect GRBs to be significantly collimated, and as discussed above, collimation reduces the energy required to power the bursts by the collimation factor f_{jet} . Knowledge of the collimation of GRBs is thus essential to inferring the energies of the bursts.

In the external shock model of GRB afterglows, the “edge” of the jet will become visible as the shock slows down and relativistic beaming decreases. Furthermore, it is expected that, as the shock slows down, it will expand laterally, initially at near the speed of light [62]. The combination of these two effects produces a steepening of the afterglow light curve (see Figures 11 and 12), although for the expected values of the parameters involved, the steepening is rather gradual [63]. However, steepening of the afterglow light curve can also occur as the external shock moves into denser circumstellar material [59,64], confounding the interpretation of the observations.

So far the observational evidence for beaming is inconclusive. For example, the lightcurve of the afterglow of GRB 990123 shows a steepening after several days that has been interpreted as due to the spreading of a jet [65,24,66], but the break is not achromatic, as would be expected if it were beamed. On the other hand, the optical and radio afterglows of GRB 990510 appear to provide stronger evidence that the burst is collimated [13]. However, the absence of large numbers of “orphan afterglows;” i.e, X-ray, optical and radio transients unassociated with GRBs [67,68,62], argues that the collimation cannot be extreme.

7 The GRB-Supernova Connection

Castander and Lamb [69] showed that the light from the host galaxy of GRB 970228, the first burst for which an afterglow was detected, is very blue. This implies that the host galaxy is undergoing copious star formation and suggests an association between GRB sources and star-forming galaxies. Subsequent analyses of the color of this galaxy [70,71] (see Figure 13) and other host galaxies (see, e.g, [24,66] have strengthened this conclusion, as has the detection of [OII] and $\text{Ly}\alpha$ emission lines from several host galaxies [16,21,72] (see Figure 14).

The inferred size ($R \lesssim 1 - 3$ kpc) and the morphology of GRB host galaxies strongly suggest that they are primarily low-mass ($M \lesssim 0.01 M_{\text{Galaxy}}$) but not necessarily sub-luminous galaxies, because of the ongoing star formation in them (most have $L \lesssim 0.01 - 0.1 L_{\text{Galaxy}}$, but some have $L \sim L_{\text{Galaxy}}$; here M_{Galaxy} and L_{Galaxy} are the mass and luminosity of a galaxy like the Milky Way). Thus, it is sometimes not fully appreciated that, while the total star

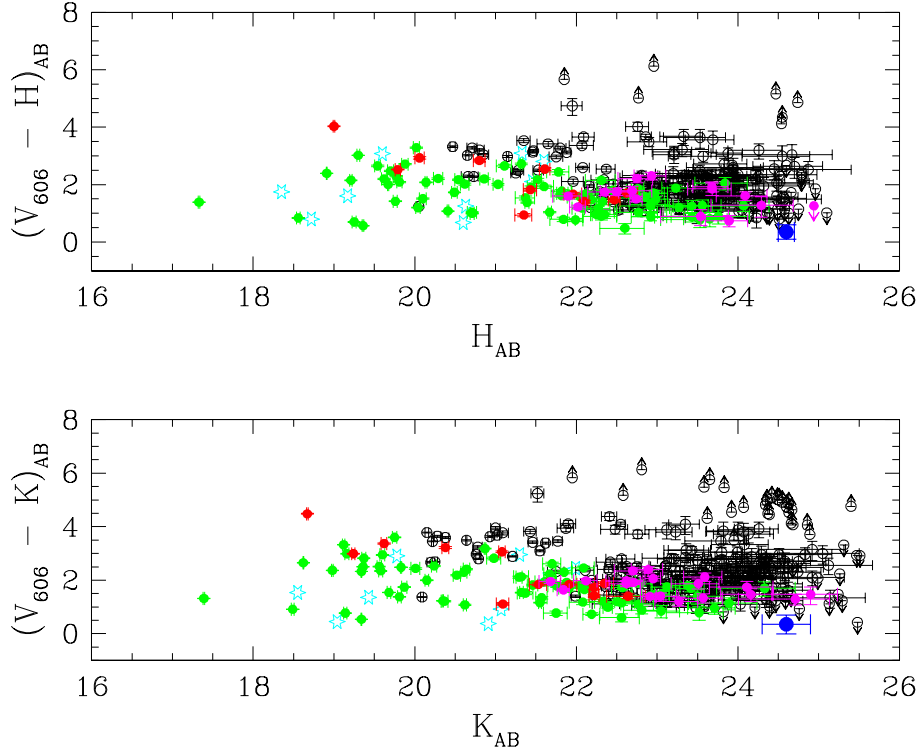


Fig. 13. HST color of the host galaxy of GRB 970228 (large filled black circle at the lower right of both panels), compared to the colors of other galaxies in the GRB field (open circles) and Hubble Deep Field (filled grey circles). [71]

formation rate in GRB host galaxies is often modest (resulting in modest [OII] and Ly α emission line strengths), the star formation rate *per unit mass* in them is very large.

Figures 6, 15 and 16 show HST WFPC2 and STIS images of the optical afterglows and host galaxies of GRBs 970228, 970508 and 990123. These images illustrate the fact that all of the GRB afterglows so far detected are coincident with bright blue regions of the host galaxies [31]. The positional coincidence between burst afterglows and the bright blue regions of the host galaxies, and the evidence for extinction by dust of some burst afterglows (see, e.g., [21,60,74], suggests that the sources of these GRBs lie near or in the

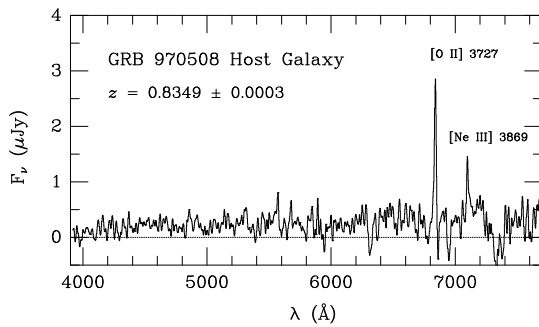


Fig. 14. Optical spectrum of the host galaxy of GRB 970508, showing [OII] 3727 \AA and [Ne III] 3869 \AA emission lines redshifted to $z = 0.83$, indicating that the host galaxy is undergoing star formation and confirming that this is the redshift of the burst [72].

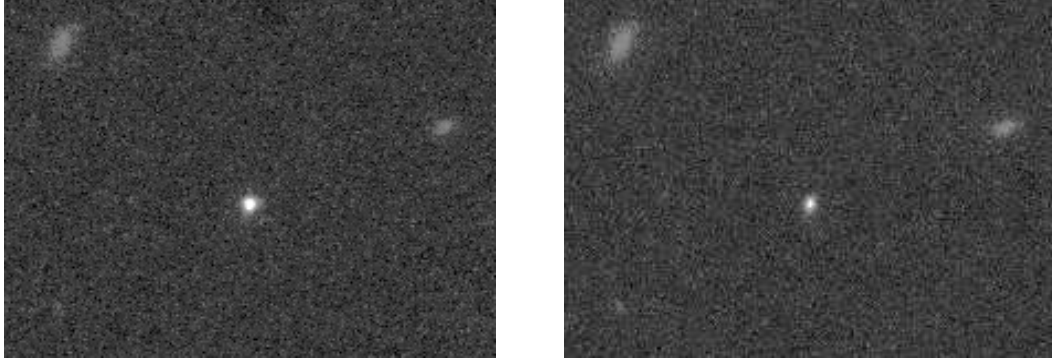


Fig. 15. Left panel: HST STIS image of the host galaxy and afterglow of GRB 970508 in 1997 June. Right panel: HST STIS image of the host galaxy and afterglow of GRB 970508 in 1997 August showing the continued fading of the optical afterglow and its coincidence with the region of star formation in the host galaxy [73].

star-forming regions themselves.

The increasingly strong evidence that the bursts detected by BeppoSAX originate in galaxies undergoing star formation, and may occur near or in the star-forming regions themselves, favors the collapsar model and disfavors the binary merger model as the explanation for long, softer, smoother bursts. Simulations of the kicks given to NS-NS and NS-BH binaries by the SNe that form them shows that most binary mergers are expected to occur well outside any galaxy [75]. This is particularly the case, given that the GRB host galaxies identified so far have small masses, as discussed earlier, and therefore low escape velocities. The fact that all of the optical afterglows of the BeppoSAX bursts are coincident with the disk of the host galaxy therefore also disfavors

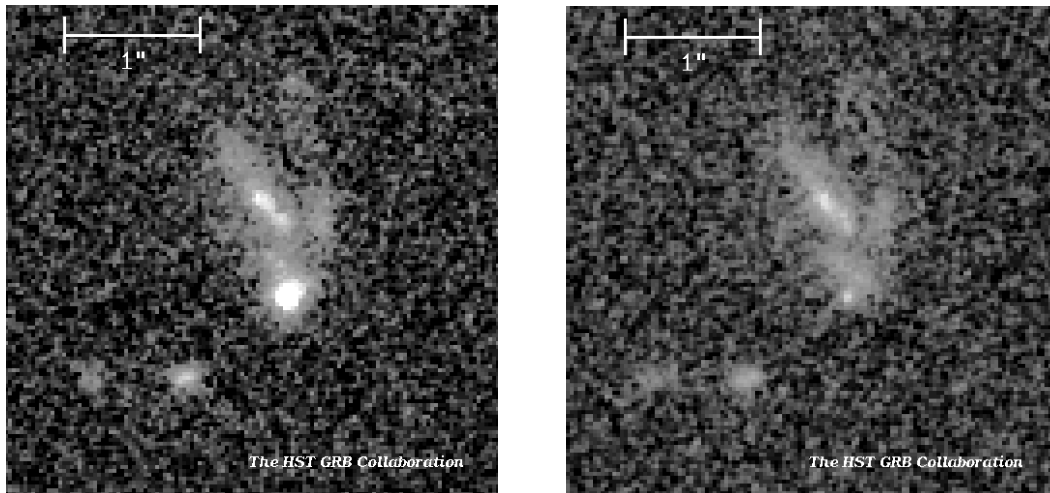


Fig. 16. HST STIS observations of the afterglow and host galaxy of GRB 990123, taken in February 1999 (left panel) and in March 1999 (right panel), showing the continued fading of the optical afterglow and its coincidence with the region of star formation in the host galaxy [66].

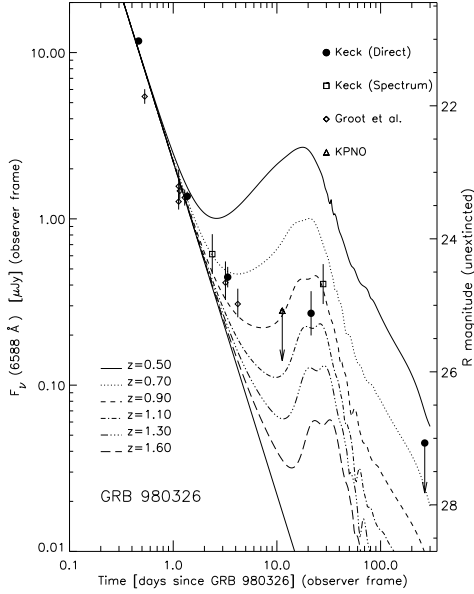


Fig. 17. R-band light curve of GRB 980326 and the sum of an initial power-law decay plus Type Ic supernova light curve for redshifts ranging from $z = 0.50$ to $z = 1.6$, showing evidence for a possible SN component. From [76]

the binary merger model as the explanation for the long, softer, smoother bursts. However, this evidence is indirect.

The discovery that the light curves and spectra of the afterglows of GRB 980326 [76] (see Figure 17) and GRB 970228 [77] (see Figures 18 and 19) appears to contain a SN component, in addition to a relativistic shock wave component, provides a more direct clue that the long, softer, smoother bursts detected by BeppoSAX are the result of the collapse of massive stars. However, the weight of this evidence is limited by the sparseness of the existing data and the small number of studied afterglows.

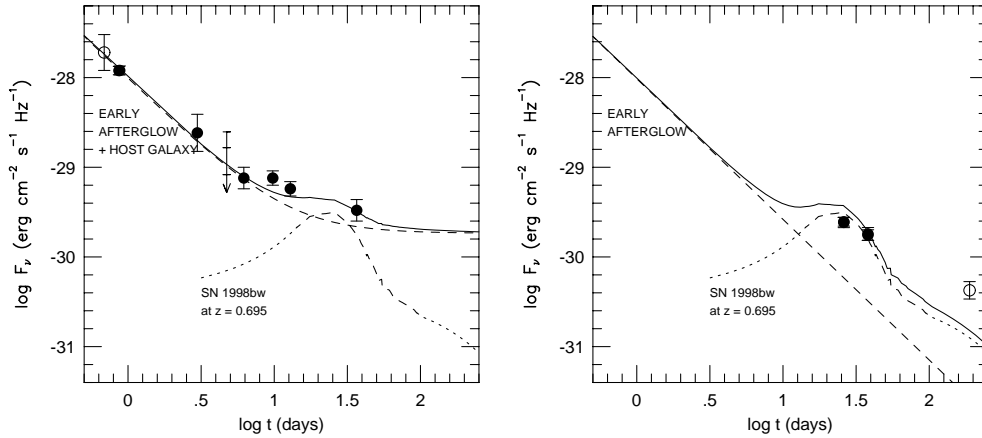


Fig. 18. Left: Light curve of GRB 970228 afterglow, showing ground-based observations. Right: Light curve of GRB 970228 afterglow, showing HST observations. Clear evidence for a second, possible SN, component in the light curve is seen, particularly in the HST observations. [77]

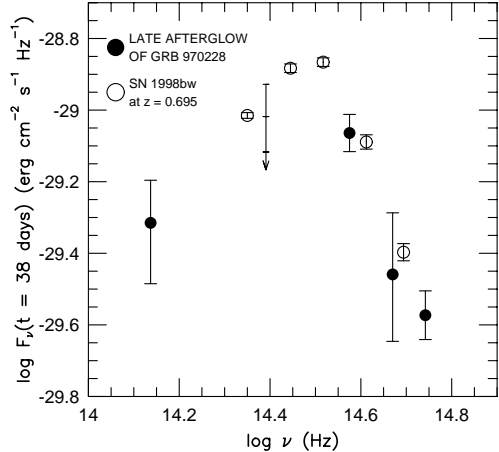


Fig. 19. Broad-band photometric spectrum of possible SN component in the late afterglow of GRB 970228 [77,78]. The filled circles and upper limits are the spectral flux densities ((SFDs) of the late afterglow after subtracting a model of the SFD of the host galaxy from Figure 18 and correcting for Galactic extinction; the unfilled circles are the I- through U-band SFDs of SN 1998bw after transforming to the redshift ($z = 0.695$) of GRB 970228 and correcting for Galactic extinction [77].

These various discoveries favor the supernova model for the long, softer, smoother GRBs that comprise 80% of GRBs and all of the bursts detected by BeppoSAX to date. However, it is important to remember that we currently have no clues whatsoever about the nature of the sources of the short, harder, more variable bursts. Even their distance scale is unknown. Happily, this situation is likely to change profoundly with the launch of HETE-2, which is capable of providing accurate, near-real time positions for both short and long bursts [79].

8 Detectability of GRBs and Their Afterglows at Very High Redshifts

One thing is now clear: GRBs are a powerful probe of the high- z universe. Lamb and Reichart [38] have calculated the limiting redshifts detectable by BATSE and HETE-2, and by *Swift*, for the seven GRBs with known redshifts and published peak photon number fluxes (see Table 1). They find that BATSE and HETE-2 would be able to detect four of these bursts (GRBs 970228, 970508, 980613, and 980703) out to redshifts $2 \lesssim z \lesssim 4$, and three (GRBs 971214, 990123, and 990510) out to redshifts of $20 \lesssim z \lesssim 30$ (see Figure 20). *Swift* would be able to detect the former four out to redshifts of $5 \lesssim z \lesssim 15$, and the latter three out to redshifts in excess of $z \approx 70$, although it is unlikely that GRBs occur at such extreme redshifts. Consequently, if GRBs occur at very high redshifts (VHRs), BATSE has probably already detected them, and future missions should detect them as well.

Lamb and Reichart [38] also show, somewhat surprisingly, that the soft X-ray, optical and infrared afterglows of GRBs are detectable out to VHRs. The reason is that, while the increase in distance and the redshifting of the spectrum tend to reduce the spectral flux in GRB afterglows in a given frequency band, cosmological time dilation tends to increase it at a fixed time of observation after the GRB, since afterglow intensities tend to decrease with time. These

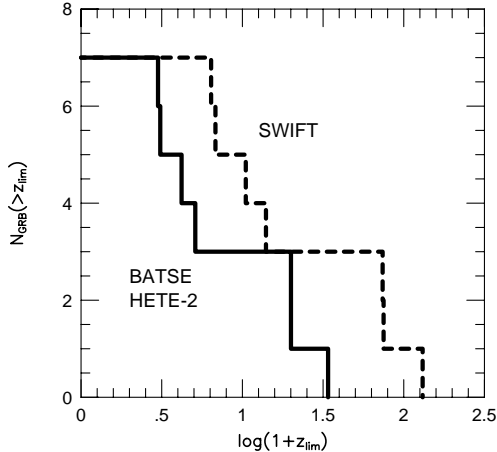


Fig. 20. Cumulative distributions of the limiting redshifts at which the seven GRBs with well-determined redshifts and published peak photon number fluxes would be detectable by BATSE and HETE-2, and by *Swift*. [38]

effects combine to produce little or no decrease in the spectral energy flux F_ν of GRB afterglows at redshifts larger than $z \approx 3$.

This result can be understood as follows. The spectral flux F_ν of GRB afterglows in a given frequency band and at a fixed time of observation after the GRB is given as a function of redshift by

$$F_\nu(\nu, t) = \frac{L_\nu(\nu, t)}{4\pi D^2(z)(1+z)^{1-a+b}}, \quad (6)$$

where $L_\nu \propto \nu^a t^b$ is the intrinsic spectral luminosity of the GRB afterglow, which we assume applies even at early times, and $D(z)$ is the comoving distance to the burst. Many afterglows fade like $b \approx -4/3$, which implies that $F_\nu(\nu, t) \propto D(z)^{-2}(1+z)^{-5/9}$ in the simplest afterglow model where $a = 2b/3$ [80]. In addition, $D(z)$ increases very slowly with redshift beyond a redshift $z \approx 3$. Consequently, there is little or no decrease in the spectral flux of GRB afterglows with increasing redshift beyond $z \approx 3$.

For example, [82] find in the case of GRB 980519 that $a = -1.05 \pm 0.10$ and $b = -2.05 \pm 0.04$ so that $1 - a + b = 0.00 \pm 0.11$, which implies no decrease in the spectral flux with increasing redshift, except for the effect of $D(z)$. In the simplest afterglow model where $a = 2b/3$, if the afterglow declines more rapidly than $b \approx 1.7$, the spectral flux actually *increases* as one moves the burst to higher redshifts!

As second example, the left panel of Figure 21 shows the K-band light curves of the early afterglow of GRB 970228 [77], as observed one day after the burst, transformed to various redshifts. The transformation involves (1) dimming the afterglow, (2) redshifting its spectrum, (3) time dilating its light curve, and (4) extinguishing the spectrum using a model of the Ly α forest. The left panel of Figure 21 shows that in this case also, the three effects nearly cancel one another out at redshifts greater than a few. Thus the afterglow of a GRB occurring at a redshift slightly in excess of $z = 10$ would be detectable at K

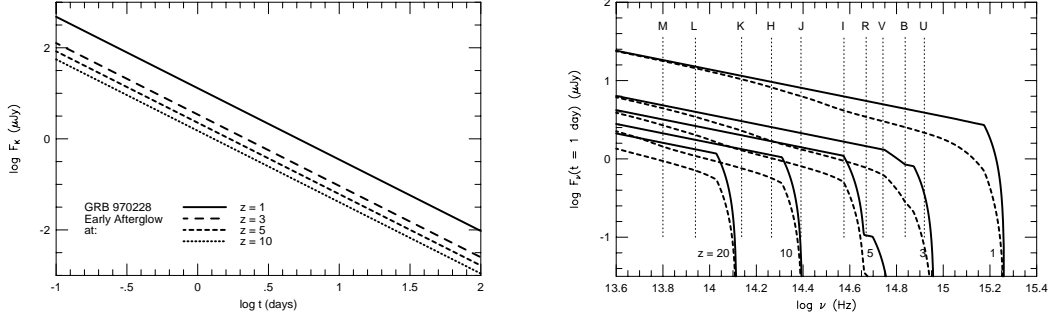


Fig. 21. Left panel: The best-fit light curve of the early afterglow of GRB 970228, transformed to various redshifts. Right panel: The best-fit spectral flux distribution of the early afterglow of GRB 970228, as observed one day after the burst, after transforming it to various redshifts, and extinguishing it with a model of the Ly α forest. The dashed curves are the same as the solid curves, but extinguished by an amount corresponding to $A_V = 1/3$ mag in the host galaxy of the burst, using an extinction curve that is typical of the interstellar medium of our own galaxy [38].

≈ 16.2 mag one hour after the burst, and at K ≈ 21.6 mag one day after the burst, if its afterglow were similar to that of GRB 970228 (a relatively faint afterglow).

The right panel of Figure 21 shows the resulting spectral flux distribution. The spectral flux distribution of the afterglow is cut off by the Ly α forest at progressively lower frequencies as one moves out in redshift. Thus the redshift distance of high-redshift ($2 \lesssim z \lesssim 5$) GRBs can readily be determined from the wavelength of the optical “dropout” in their afterglow spectrum and of very high redshift ($z \gtrsim 5$) GRBs from the wavelength of the infrared “dropout,” in their afterglow spectrum [81,38]. Figure 22 shows the visibility of any SN remnant, as a function of redshift.

These results show that, if GRBs occur at very high redshifts, both they and their afterglows would be detectable.

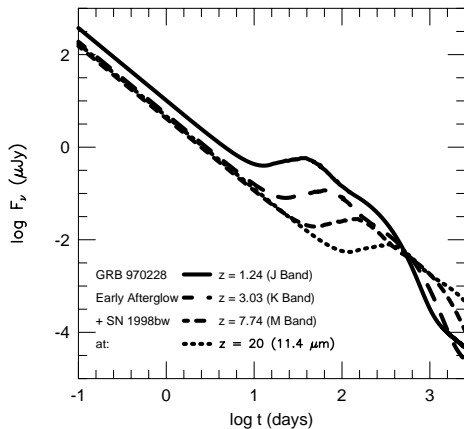


Fig. 22. Light curves of GRB afterglows, with SN components superimposed, at various redshifts [38].

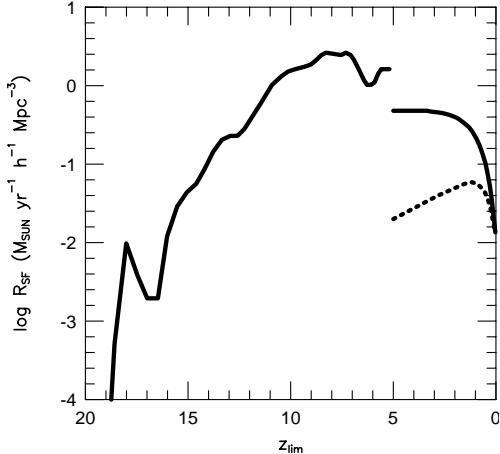


Fig. 23. The cosmic star formation rate (SFR) R_{SF} as a function of redshift z . The solid curve at $z < 5$ is the SFR derived by [84]; the solid curve at $z \geq 5$ is the SFR calculated by [86] (the dip in this curve at $z \approx 6$ is an artifact of their numerical simulation). The dotted curve is the SFR derived by [83]. From [38].

9 GRBs as a Probe of the Very High Redshift Universe

Observational estimates (see e.g., [83,84]) suggest that the star-formation rate (SFR) in the universe was an order of magnitude larger at a redshift $z \approx 1$ than it is today. The data at higher redshifts from the Hubble Deep Field (HDF) in the North suggest a peak in the SFR at $z \approx 1 - 2$ [83], but the actual situation is highly uncertain. Theoretical calculations show that the birth rate of Pop III stars produces a peak in the SFR in the universe at redshifts $16 \lesssim z \lesssim 20$, while the birth rate of Pop II stars produces a much larger and broader peak at redshifts $2 \lesssim z \lesssim 10$ [85–87]. Therefore one expects GRBs to occur out to at least $z \approx 10$ and possibly $z \approx 15 - 20$, redshifts that are far larger than those expected for the most distant quasars. Consequently GRBs may be a powerful probe of the star-formation history of the universe, and particularly of the SFR at VHRs.

Figure 23 shows the SFR versus redshift from a phenomenological fit [84] to the SFR derived from sub-millimeter, infrared, and UV data at redshifts $z < 5$, and from a numerical simulation by [86] at redshifts $z \geq 5$. The numerical simulations indicate that the SFR increases with increasing redshift until $z \approx 8$, at which point it levels off. The smaller peak in the SFR at $z \approx 18$ corresponds to the formation of Population III stars, brought on by cooling by molecular hydrogen.

Lamb and Reichart [38] have calculated the expected number of GRBs as a function of redshift, assuming (1) that the GRB rate is proportional to the SFR and (2) that the SFR is that given in Figure 23. The first assumption may underestimate the GRB rate at VHRs since it is generally thought that the initial mass function will be tilted toward a greater fraction of massive stars at VHRs because of less efficient cooling due to the lower metallicity of the universe at these early times. There is a mis-match of about a factor of three between the $z < 5$ and $z \geq 5$ regimes. However, estimates of the star formation rate are uncertain by at least this amount in both regimes. Lamb

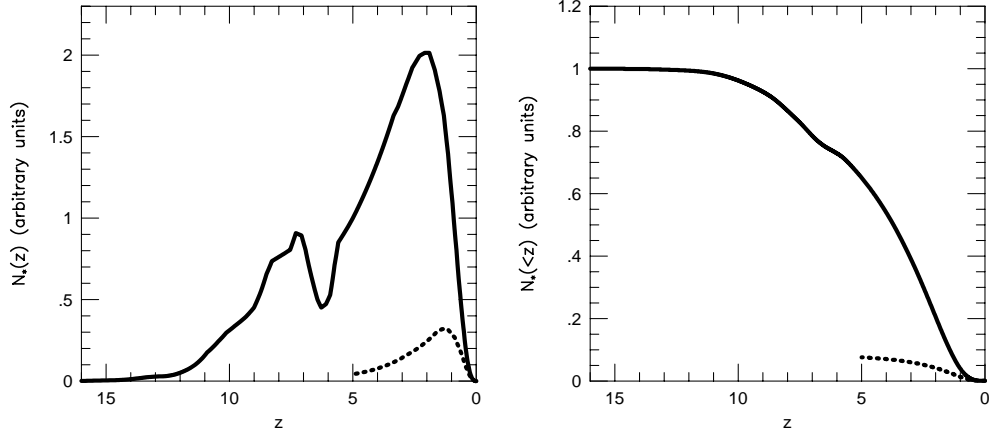


Fig. 24. Left panel: The number N_* of stars expected as a function of redshift z (i.e., the SFR from Figure 1, weighted by the differential comoving volume, and time-dilated) assuming that $\Omega_M = 0.3$ and $\Omega_\Lambda = 0.7$. Right panel: The cumulative distribution of the number N_* of stars expected as a function of redshift z . Note that $\approx 40\%$ of all stars have redshifts $z > 5$. The solid and dashed curves in both panels have the same meanings as in Figure 1. From [38]

and Reichart [38] have therefore chosen to match the two regimes smoothly to one another, in order to avoid creating a discontinuity in the GRB peak flux distribution that would be entirely an artifact of this mis-match. Figure 24 shows their results.

The left panel of Figure 24 shows the number $N_*(z)$ of stars expected as a function of redshift z (i.e., the SFR, weighted by the co-moving volume, and time-dilated) for an assumed cosmology $\Omega_M = 0.3$ and $\Omega_\Lambda = 0.7$ (other cosmologies give similar results). The solid curve corresponds to the star-formation rate in Figure 23. The dashed curve corresponds to the star-formation rate derived by [83]. This figure shows that $N_{GRB}(z) [\propto N_*(z)]$ peaks sharply at $z \approx 2$ and then drops off fairly rapidly at higher z , with a tail that extends out to $z \approx 12$. The rapid rise in $N_*(z)$ out to $z \approx 2$ is due to the rapidly increasing volume of space. The rapid decline beyond $z \approx 2$ is due almost completely to the “edge” in the spatial distribution produced by the cosmology. In essence, the sharp peak in $N_*(z)$ at $z \approx 2$ reflects the fact that the SFR is fairly broad in z , and consequently, the behavior of $N_*(z)$ is dominated by the behavior of the co-moving volume $dV(z)/dz$; i.e., the shape of $N_*(z)$ is due almost entirely to cosmology. The right panel in Figure 24 shows the cumulative distribution $N_*(> z)$ of the number of stars expected as a function of redshift z . The solid and dashed curves have the same meaning as in the upper panel. This figure shows that $\approx 40\%$ of all stars have redshifts $z > 5$. Since GRBs are detectable at these VHRs and their redshifts may be measurable from the absorption-line systems and the Ly α break in the afterglows, if the GRB rate is proportional to the SFR, then GRBs could provide unique information about the star-formation history of the VHR universe [38].

GRB afterglows can also serve as a probe of many other important aspects of the VHR universe [38]. The absorption-line systems and the Ly α forest visible in the spectra of GRB afterglows can be used to trace the evolution of metallicity in the universe, and to probe the large-scale structure of the universe at very high redshifts. Finally, measurement of the Ly α break in the spectra of GRB afterglows can be used to constrain, or possibly measure, the epoch at which re-ionization of the universe occurred, using the Gunn-Peterson test [88].

10 Conclusions

The discoveries that GRBs have X-ray, optical and radio afterglows have connected the study of GRBs to the rest of astronomy, and revolutionized the field. We now know that the sources of most (and perhaps all) GRBs lie at cosmological distances, and that the bursts are among the most energetic and luminous events in the universe. There is increasing indirect evidence that the long, softer, smoother GRBs detected by BeppoSAX are associated with the star-forming regions of galaxies, and tantalizing direct evidence that these bursts are connected to core collapse supernovae. If these GRBs are due to the collapse of massive stars, they may be a powerful probe of the very high redshift universe.

Acknowledgments

David Schramm was a wonderfully enthusiastic and supportive colleague. His scientific interests ranged over much of astrophysics, including the mysterious phenomenon of gamma-ray bursts. I am sure that he would have been excited about recent observational evidence that appears to link GRBs and one of his favorite subjects, supernovae; and delighted that GRBs may be a powerful probe of the early universe, a topic to which he contributed so much. This work was supported in part by NASA contract NAGW-4690.

References

- [1] Klebesadel R. W., Strong I. B. & Olson R. A. *ApJ* **182** (1973) L85.
- [2] Paciesas W. S. et al., *ApJS* **122** (1999) 465.
- [3] Lamb, D. Q., Graziani, C. & Smith, I. A. *ApJ* **413** (1993) (1993) L11.

- [4] Kouveliotou, C., et al., *ApJ* **413** (1993) L101.
- [5] Band, D., et al., *ApJ* **413** (1993) 281.
- [6] Schaefer, B. E., et al., *ApJS* **92** (1994) 285.
- [7] Meegan C. A. et al., *Nature* **355** (1993) 143.
- [8] Lamb D. Q. *PASP* **107** (1995) 1152.
- [9] Paczynski B. *PASP* **107** (1995) 1166.
- [10] Costa E. et al., *IAU Circular No.* 6576 (1997).
- [11] van Paradijs, J., et al., *Nature* **386** (1997) 686.
- [12] Frail D. A. et al., *Nature* **389** (1997) 261.
- [13] Kulkarni, S. R., et al. *Gamma-Ray Bursts (2000) AIP Conference Proceedings* R.M. Kippen, R. Mallozzi, and G. Fishman, eds., New York, AIP, in press.
- [14] Costa, E. *Nature* **387** (1997) 783.
- [15] Sahu, K. C., et al., *Nature* **387** (1997) 476.
- [16] Metzger, M., et al., *Nature* **387**(1997) 878.
- [17] Akerlof, C. et al., *Nature* **398**(1999) 400.
- [18] Costa, E. *A&A Suppl* **138** (1999) 425.
- [19] Frail, D. A., et al., *Gamma-Ray Bursts (2000)* R.M. Kippen, R. Mallozzi, and G. Fishman eds., *AIP Conference Proceedings* New York, AIP, in press.
- [20] Djorgovski, S. G., et al. *GCN Report No.* 289 (1999).
- [21] Kulkarni, S. R., et al. *Nature* **395**(1998) 663.
- [22] Djorgovski, S. G., et al. *GCN Report No.* 189 (1999).
- [23] Djorgovski, S. G., et al. *ApJ* **508** (1998) L17.
- [24] Kulkarni, S. R., et al. *Nature* **398**(1999) 389.
- [25] Vreeswijk, P. M., et al. *GCN Report No.* 324 (1999).
- [26] Galama, T. J., et al., *GCN Report No.* 388 (1999).
- [27] Fenimore, E. E. et al. *Nature* **366** (1993) 40.
- [28] Totani, T. *ApJ* **486** (1997) L71.
- [29] Totani, T. *ApJ* **511** (1999) 41.
- [30] Wijers, R. & Galama, T. J. *ApJ* **523** (1999) 177.
- [31] Hogg, D. W., & Fruchter, A. S. *ApJ* **520** (1999) 54.

- [32] Schmidt, M. *Gamma-Ray Bursts* (2000) R. M. Kippen, R. Mallozzi, and G. Fishman, eds., *AIP Conference Proceedings* New York, AIP, in press.
- [33] Cappellaro, E. et al. *A&A* **322** (1997) 431.
- [34] Lamb, D. Q. *A&A Suppl.* **138** (1999) 607.
- [35] Loredó, T. J. & Wasserman, I. *ApJ* **502** (1998) 75.
- [36] Loredó, T. J. & Wasserman, I. *ApJ* **502** (1998) 108.
- [37] Wasserman, I. *ApJ* 394 (1992) 565.
- [38] Lamb, D. Q. & Reichart, D. E. *ApJ* (1999), in press.
- [39] Norris, J. P. et al. *ApJ* 424 (1994) 540.
- [40] Fenimore, E. E. & Bloom, J. S. *ApJ* 453 (1994) 25.
- [41] Stern, B. E. *ApJ* 464 (1996) L111.
- [42] Stern, B. E., Poutanen, J. & Svensson, R. *ApJ* 510 (1999) 312.
- [43] Mallozzi, R. S., Pendleton, G. N. & Paciesas, W. S. *ApJ* 471 (1999) 636.
- [44] Woosley, S. E. *ApJ* **405** (1993) 273.
- [45] Woosley, S. E. *Gamma-Ray Bursts* C. Kouveliotou, M. Briggs, G. Fishman, eds. AIP Conference Proceedings, Vol. 384, New York, AIP, 1995, p. 709
- [46] Paczyński, B. *ApJ* **494** (1998) L45.
- [47] MacFadyen, A. I., & Woosley, S. E. *ApJ* **524** (1999) 262.
- [48] MacFadyen, A. I., Woosley, S. E., & Heger A. *ApJ* (1999), submitted (astro-ph/9910034).
- [49] Khokhlov, A. M. et al. *ApJ* **524** (1999) L107.
- [50] Wheeler, J. C., et al. *ApJ* (2000), in press (astro-ph/9909293).
- [51] Paczyński, B. *ApJ* **308** (1986) L43.
- [52] Narayan, R., Paczyński, B., & Piran, T. *ApJ* **395** (1992) L83.
- [53] Mészáros, P. & Rees, M. J. *ApJ* **397** (1993) 570.
- [54] Woosley, S. E. & MacFadyen A. I. *A&A Suppl.* **138** (1999) 499.
- [55] Dermer, C. 1999, *A&A Suppl.* **138** (1999) 519.
- [56] Fenimore, E. E., Ramirez-Ruiz, E. & Wu, Bobing *Gamma-Ray Bursts: The First Three Minutes* J. Poutanen and R. Svensson, eds. *ASP Conference Series* San Francisco, ASP, **190** (1999), p. 67.
- [57] Waxman, E. 1997, *ApJ* **489** (1997) L33.

- [58] Sari, R., Piran, T. and Narayan, R. *ApJ* **497** (1998) L17.
- [59] Chevalier, R. A. & Li, Z.-Y. *ApJ* **520** (1999) L29.
- [60] Lamb, D. Q., Castander, F. J., & Reichart, D. E. *A&A Suppl.* **138** (1999) 479.
- [61] Wheeler, J.C. 1999, *Cosmic Explosions*, S. Holt and W. Zhang, eds. *AIP Conference Proceedings* New York, AIP, in press. (astro-ph/9912403).
- [62] Rhoads, J. E. *ApJ* **487** (1997) L1.
- [63] Moderski, R., Sikora, M. & Bulik, T. *ApJ* (1999), in press (astro-ph/904310).
- [64] Chevalier, R. A. & Li, Z.-Y. *ApJ* (1999), in press (astro-ph/9908272).
- [65] Mészáros, P. & Rees, M. J., *ApJ* **476** (1997) 232.
- [66] Fruchter, A. S., et al. *ApJ* **519** (1999) L13.
- [67] Greiner, J., et. al. *A&A Suppl.* **138** (1999) 441.
- [68] Grindlay, J. E. *ApJ* **510** (1999) 710.
- [69] Castander, F. J. & Lamb, D. Q. *Gamma-Ray Bursts* C. A. Meegan, R. D. Preece, & T. M. Koshut eds., New York: AIP, 1998, p. 520.
- [70] Castander, F. J. & Lamb, D. Q. *ApJ* **523** (1999) 593.
- [71] Fruchter, A. S., et al. *ApJ* **516** (1999) 683.
- [72] Bloom, J. S., Djorgovski, S. G., Kulkarni, S. R. & Frail, D. A. *ApJ* **507** (1998) L25.
- [73] Pian, E., et al. *ApJ* **492** (1998) L103.
- [74] Reichart, D. E. *ApJ* **495** (1998) L99.
- [75] Bulik, T. & Belczyński, K. & Zbijewski, W. 1999, *A&A Suppl.* **138** (1999) (483).
- [76] Bloom, J. S., et al. *Nature* **401** (1999) 453.
- [77] Reichart, D. E. 1999a, *ApJ* **521** L111.
- [78] Reichart, D. E., Lamb, D. Q. & Castander, F. J. *Gamma-Ray Bursts* R. M. Kippen, R. Mallozzi, and G. Fishman, eds., *AIP Conference Proceedings* New York, AIP, 2000, in press.
- [79] Lamb, D. Q. 2000, *Cosmic Explosions* S. Holt and W. Zhang, eds. *AIP Conference Proceedings* New York, AIP, in press.
- [80] Wijers, R. A. M. J., Rees, M. J., & Mészáros, P. *MNRAS* **288** (1997) L51.
- [81] Fruchter, A. S. *ApJ* **512** (1999) L1.
- [82] Halpern, J. P. *ApJ* **517** (1999) L105.
- [83] Madau, P., Pozzetti, L., & Dickinson, M. *ApJ* **498** 106.

- [84] Rowan-Robinson, M. *Astroph. & Space Sci.* (1999), in press (astro-ph/9906308).
- [85] Ostriker, J. P., & Gnedin, N. Y. *ApJ* **472** (1996) L63.
- [86] Gnedin, N. Y., & Ostriker, J. P. *ApJ* **486** (1997) 581.
- [87] Valageas, P., & Silk, J. *A&A*, **347** (1999) 1.
- [88] Gunn, J. E. & Peterson, B. A. *ApJ* **142** (1965) 1633.